

Cycloidal Quasi-Direct Drive Actuator Designs with Learning-based Torque Estimation for Legged Robotics

Alvin Zhu^{1*}, Yusuke Tanaka^{2*}, Fadi Rafeedi² and Dennis Hong²

Abstract—This paper presents a novel approach through the design and implementation of Cycloidal Quasi-Direct Drive actuators for legged robotics. The cycloidal gear mechanism, with its inherent high torque density and mechanical robustness, offers significant advantages over conventional designs. By integrating cycloidal gears into the Quasi-Direct Drive framework, we aim to enhance the performance of legged robots, particularly in tasks demanding high torque and dynamic loads, while still keeping them lightweight. Additionally, we develop a torque estimation framework for the actuator using an Actuator Network, which effectively reduces the sim-to-real gap introduced by the cycloidal drive’s complex dynamics. This integration is crucial for capturing the complex dynamics of a cycloidal drive, which contributes to improved learning efficiency, agility, and adaptability for reinforcement learning.

I. INTRODUCTION

Agile and dynamic locomotion in legged robots has been a longstanding challenge in robotics, requiring actuators that can deliver both dynamic torque control and high responsiveness, such as Direct Drive (DD) [1], [2] and Quasi-Direct Drive (QDD) [3] systems. However, integrating the gearbox into a confined space with conventional planetary, spur gear, and belt drive mechanisms is challenging without sacrificing gear load capacity since they are less resilient to significant impulse load, such as those experienced during a fall.

Cycloidal gear mechanisms offer rigidity and superior gear teeth stress distribution [4], allowing the design to be compact but promising adequate mechanical strength and minimal backlash [5], [6]. Integrating a cycloidal gearbox into a QDD system, the Cycloidal Quasi-Direct Drive (C-QDD) can enhance performance, especially in applications that demand high torque and dynamic load handling. However, cycloidal gears introduce nonlinearities in the torque output of the C-QDD, which can impact applications like reinforcement learning (RL) due to unmodeled dynamics in the actuator model during simulation [7]. Thus, modeling and estimating the C-QDD torque output is essential to bridging the sim-to-real gap [8].

Data-driven approaches, such as the Actuator Net [8] for modeling C-QDD, offer advantages since it is challenging to measure and account for manufacturing tolerances, to which cycloidal gears are particularly sensitive [9]. The significance of learning-based modeling lies in its ability to generalize across different operating conditions while maintaining high accuracy using only actuation history data [10].

¹A. Zhu is with the Department of Computer Science and Electrical Engineering, ²Y. Tanaka, F. Rafeedi, and D. Hong are with the Department of Mechanical and Aerospace Engineering, UCLA, Los Angeles, CA, USA. {alvister88, yusuketanaka, frafeedi, dennishong}@ucla.edu. *A. Zhu and Y. Tanaka assert joint first authorship.

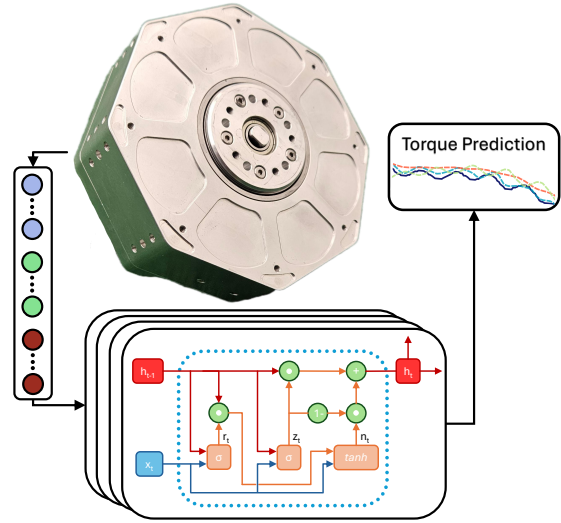


Fig. 1: Proposed cycloidal gear quasi-direct drive actuator and the torque estimation framework.

This paper presents a QDD actuator with a 10:1 cycloidal gearbox for legged robots. We also present a gated recurrent unit (GRU) based torque estimation framework to model nonlinearities induced by the cycloidal gear such as the torque ripple. The C-QDD actuator is benchmarked and the performance of the GRU torque estimation framework is evaluated experimentally.

The contributions of this paper are:

- 1) **Design of a Cycloidal Quasi-Direct Drive Actuator:** We introduce a cycloidal quasi-direct drive actuator design tailored for dynamic locomotion and demanding climbing [11].
- 2) **Torque estimation framework:** We develop a GRU-based torque estimation framework that can predict non-linear, high-frequency features such as torque ripple to reduce the sim-to-real gap effectively.
- 3) **Hardware verifications:** We verify and analyze the C-QDD performances, backdrivability, and the torque estimation framework on hardware.

II. RELATED WORKS

A. Actuation Mechanism in Legged Robotics

Traditional robotic actuators are designed to be rigid, enabling precise position control [12], [13]. However, rigid and non-backdrivable actuators are not ideal for dynamic and agile-limbed systems [14], [15], as compliance and torque control are essential for legged robots [3]. Various types of

actuators have been proposed to enable accurate force control and safe interaction with the environment in legged robots. Compliant actuators, such as series elastic actuators [16] and variable stiffness actuators [17], address these challenges by introducing a compliant element between the motor and the output. However, these actuators require extensive modeling, optimization, and complex control algorithms. Recently, QDD actuators have gained popularity in legged robots [18]. These proprioceptive actuators offer high torque fidelity and reduce reflected inertia, making them an ideal choice for legged robots. DD[19] and QDD [20] actuators have been foundational in achieving precise torque control and high responsiveness in legged robots. DD actuators are praised for their simplicity and torque transparency, which minimize mechanical impedance [3] and allow for accurate force control. In contrast, QDD actuators integrate gear reductions with direct drive principles, balancing torque amplification and control transparency [21]. Recent advancements in QDD technology have focused on optimizing gear ratios and reducing backlash, further enhancing the actuator’s performance in high-impact environments [22].

B. Cycloidal Gear Mechanisms

Cycloidal gears have gained popularity as an alternative to planetary gears in legged robots due to their capacity to withstand large dynamic loads and frequent impacts [5], [23]. Additionally, cycloidal gearboxes are compact and typically exhibit less backlash compared to planetary gears [24]. However, despite these advantages, cycloidal gears also present several drawbacks stemming from the unique dynamics of the system [25]. These include torque ripple, backlash, and unintended vibrations caused by the eccentricity of the rotors, which can be compensated by using data-driven modelling.

C. Actuator Modeling

Advanced actuator modeling and control are essential for managing the complexities of modern actuator designs, which introduce significant non-linearities and dynamic variations [26]. Traditional control methods often struggle with these challenges, but data-driven approaches, such as Actuator Networks, have proven effective in improving real-time control and prediction accuracy. By utilizing machine learning to model actuator dynamics based on offline data, Actuator Networks help bridge the sim-to-real gap in legged robots, as demonstrated by ETH Zurich’s ANYmal equipped with Series Elastic Actuators (SEA), enhancing both adaptability and performance [8]. Moreover, integrating RL with these actuator designs enable robots to optimize control policies for complex tasks autonomously. However, RL still faces challenges such as unsafe exploration and sim-to-real transfer difficulties [27], [28]. Actuator Networks address these challenges by improving the accuracy of actuator models, thereby aiding in the transferability of learned policies from simulation to real-world environments [29].

III. CYCLOIDAL GEAR QUASI-DIRECT DRIVE MECHANISMS

The use of cycloidal gears in low gear ratio and high backdrivability actuators introduces unique challenges to the design of cycloidal mechanisms. In this section, we will discuss the design principles behind C-QDD actuators, focusing on how these parameters are optimized to achieve the desired performance characteristics.

A. Sizing of Cycloidal and Planetary Gears

Here, we compare the load capacity of our cycloidal gears with that of traditional planetary gears, which are commonly used in proprioceptive actuators [5]. The gearbox is integrated into the stator’s interior to maintain a compact design, limiting the maximum allowable pitch diameter for the cycloidal gear. A compound planetary gear can achieve a gear ratio of 10 while remaining compact enough to fit within the stator. One such configuration includes a sun gear with 12 teeth, planet gears with 36 and 22 teeth, and a ring gear with 70 teeth.

For the given peak loads, the torque capacity of our cycloidal gear is limited by the output pins. In contrast, tooth bending and surface strength constrain the compound planetary gear’s load capacity. To support the peak torque of 120 Nm from the C-QDD, a planetary gear system would require six planets. This, in addition to not fitting within design constraints, will experience surface failure at the actuator’s rated continuous torque levels of 40 Nm for a module 1 gear with a thickness of 12 mm.

The cycloidal gear’s output pins are precision shoulder screws made of 18-8 stainless steel, positioned 19.5 mm from the center of rotation. This configuration allows for a maximum torque of 59.13 Nm per pin, providing a total of 295.65 Nm of torque.

B. Cycloid profiles and eccentricity

The cycloid profile is controlled by the pitch diameter, $2Z_r$, eccentricity, Z_e , and outer pin diameter, Z_p , in Fig. 2b.

The eccentricity of the cycloid gear induces an imbalance in gear inertia, which leads to undesired vibrations. To mitigate this effect, a counterbalancing disk is incorporated into the gearbox. The cycloid gear transmission ratio determines the number of counter disks required, Z_R , defined as:

$$Z_R = \frac{-Z_{np}}{Z_{np} - Z_{nt}} = -Z_{nt} \quad (1)$$

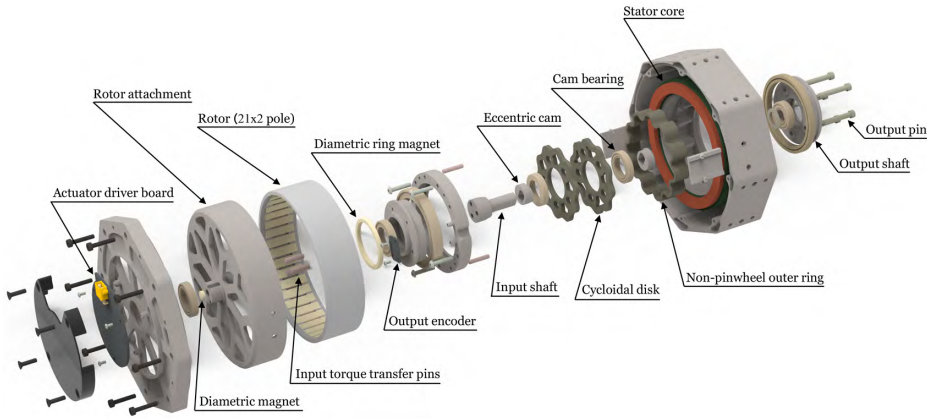
where Z_{np} represents the number of outer pins, and Z_{nt} denotes the number of teeth on the cycloid gear. The number of disks, N_Z required is denoted as

$$Z_R = 2k \quad (\text{even number}), \quad N_Z = 2 \quad (2)$$

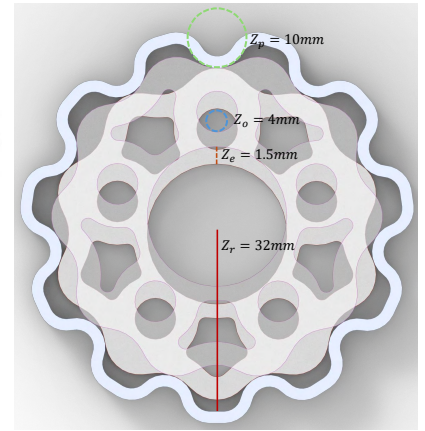
$$Z_R = 2k + 1 \quad (\text{odd number}), \quad N_Z = 3 \quad (3)$$

$$k \in \mathbb{Z}, \quad k \geq 2 \quad (4)$$

Here, k is a positive integer, and N_{disks} is the number of counterbalancing disks.



(a) An exploded view of the C-QDD design.



(b) Cycloidal disk and ring profile with Z_r as pitch radius, Z_e as eccentricity, Z_o as output pin diameter, and Z_p as outer pin diameter.

Fig. 2: C-QDD actuator design and cycloidal profiles.

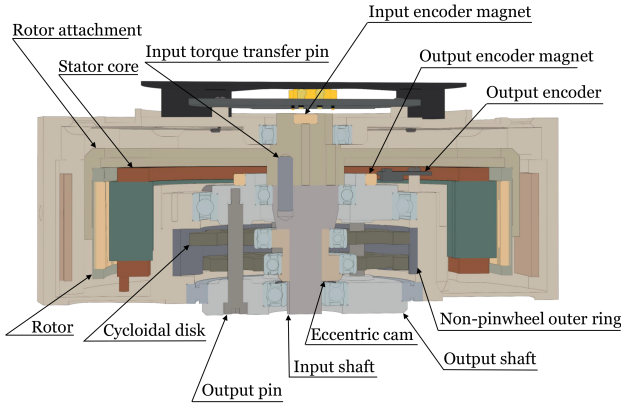


Fig. 3: A cross-section view of the C-QDD design.

Two disks are sufficient to balance the inertia statically. However, to ensure dynamic stability, three disks are necessary to compensate for dynamic imbalances that may arise due to material deformation and manufacturing inaccuracy [9]. In the C-QDD design, two counter disks are employed as the transmission ratio, $Z_R = 10$, necessitates the use of an even number of disks and significantly increases reflected inertia, impacting the backdrivability of the actuator. The dynamic imbalance of the cycloid disk contributes to oscillations and torque ripples, which are compensated for through the torque estimation framework in Section V-C.

C. Non-Pinwheel Cycloid Ring

In the C-QDD, a non-pinwheel outer cycloid ring is employed, instead of the conventional pinwheel designs [30], [31]. Both the cycloid disks and the outer rings are manufactured from 4140 alloy steel, known for their superior rigidity, wear resistance, and dimensional stability compared to the 7075 aluminum housing. Pinwheel designs traditionally utilize dowel pins embedded in the housing, which can present manufacturing challenges. Drilling pinholes directly into the housing necessitates tight tolerance control. C-QDD resolves

these challenges by utilizing independent solid rings, which may accommodate better manufacturing tolerances among the cycloid disks, eccentric cams, and other components. The cycloid disks and rings are machined from tight tolerance ground flat stock using a wire EDM at $\pm 2\ \mu\text{m}$ tolerance.

IV. C-QDD SYSTEM DYNAMICS AND TORQUE ESTIMATION

To model the dynamics of the C-QDD, we employ a deep learning-based torque estimation framework, mitigating challenges such as force sensorless torque control, cycloid nonlinear ripple, and high-frequency oscillations. The torque estimation framework, depicted in Fig. 4, processes the actuator's state feedback to produce torque predictions.

A. Torque Estimation Framework

The proposed torque estimation framework utilizes a Gated Recurrent Unit (GRU) [32] based architecture to model the actuator's dynamic behavior through the joint states. Over the time history horizon, L , two different sets of input vectors are defined as:

- **PV-GRU:** $\mathbf{X}_{v_t} \in \mathbb{R}^{2L}$, where $\mathbf{X}_{v_t} = [\mathbf{q}_e, \dot{\mathbf{q}}]^\top$
- **PVA-GRU:** $\mathbf{X}_{a_t} \in \mathbb{R}^{3L}$, where $\mathbf{X}_{a_t} = [\mathbf{q}_e, \dot{\mathbf{q}}, \ddot{\mathbf{q}}]^\top$

The joint error \mathbf{q}_e is calculated as $\mathbf{q}_e = \mathbf{q}_{\text{ref}} - \mathbf{q}$, where \mathbf{q}_{ref} is the reference trajectory given and \mathbf{q} is the current joint position. The $\dot{\mathbf{q}} \in \mathbb{R}^L$ represents the joint velocity over a history of L timesteps. The normalization of the inputs ensures consistent model performance and prevents scale imbalances that could hinder training.

The decision to include acceleration, $\ddot{\mathbf{q}} \in \mathbb{R}^L$, in the PVA-GRU variant arises to capture high-frequency, nonlinear torque dynamics more effectively—particularly phenomena such as torque ripple and oscillatory behavior. Such high-frequency dynamics require higher-order state information to enhance predictive accuracy, especially in regimes where position and velocity alone may be insufficient, as indicated by prior work [8]. This will be further demonstrated through empirical validation in Section V.

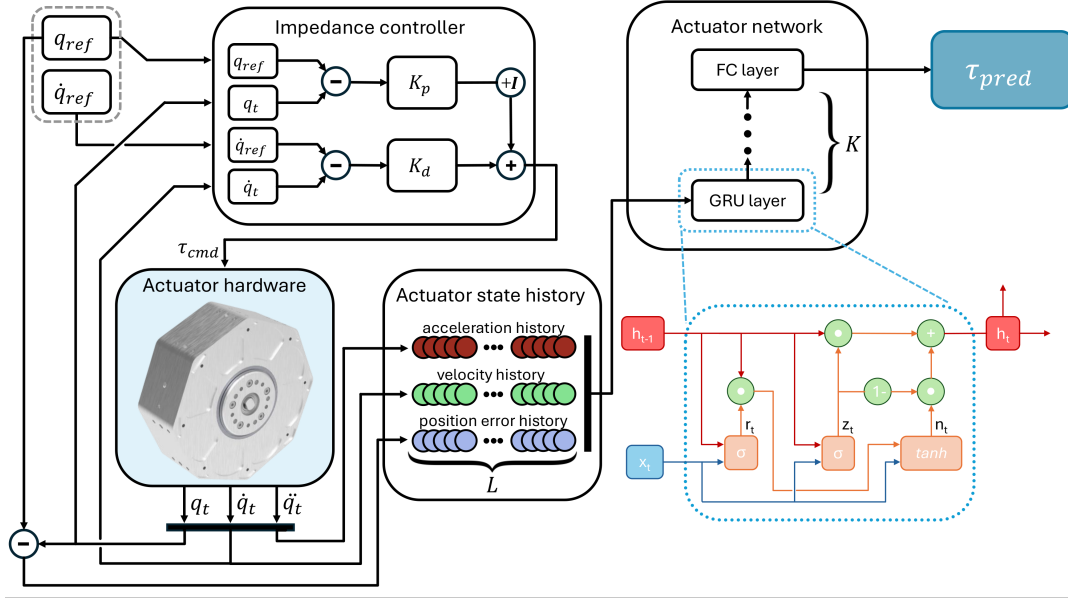


Fig. 4: Overview of the Torque Estimation Framework for torque estimation.

The GRU architecture was selected due to its capability to capture temporal dependencies efficiently, even across sequences of varying lengths. By maintaining an internal memory, the GRU processes historical state information x_t along with the hidden state h_{t-1} to iteratively update its predictions, thus enabling the network to learn long-term dependencies that are critical for accurately predicting high-frequency torque ripple.

B. System Identification and Training

The network is trained to minimize the error between the predicted torque and the actual measured torque, τ_{pred} . Supervised learning is employed using historical data collected under diverse operating conditions of the C-QDD actuator, capturing a wide range of dynamic behaviors.

The training pipeline uses the Adam optimizer with an initial learning rate of 0.0001, coupled with a One Cycle Learning Rate (LR) scheduler for efficient convergence [33], [34]. This approach dynamically adjusts the learning rate to prevent overfitting while fine-tuning model performance during the final training stages.

Key hyperparameters were tuned to optimize performance:

- History size ($L = 30$)—providing sufficient temporal information to capture high-frequency dynamics.
- Number of GRU layers ($K = 4$)—striking a balance between model complexity and computational efficiency.
- Batch size = 64.

The parameter L was determined by considering the dataset’s sampling rate and the observed torque ripple frequency range. This ensures that the network receives enough historical data to capture the actuator’s intricate dynamics. Similarly, K was adjusted to enable the network to model higher-order features while maintaining computational efficiency effectively, crucial for real-time applications.

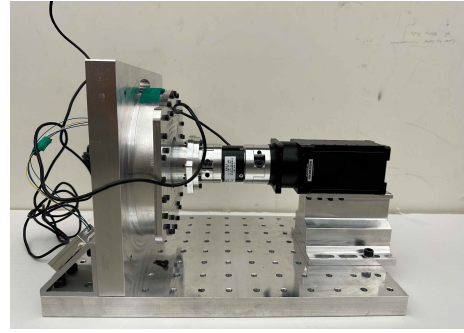


Fig. 5: C-QDD actuator performance benchmark testbed.

V. HARDWARE VERIFICATION AND ANALYSIS

In this section, we benchmark the C-QDD actuator’s attributes and performance based on metrics critical to legged robots. These parameters include its torque and position control bandwidth, as well as its backdriving torque to highlight its ability to absorb impacts. The test set-up for our experiments is shown in Fig. 5. In this test setup, the C-QDD’s chassis is fixed, and the output is directly connected to a torque sensor, which is then connected to a Dynamixel Pro (H54-200-S500-R) servo motor. For tests requiring a high-impedance output setup, the servomotor is swapped with a rigid connection.

A. C-QDD Mechanical and Electrical Performance

C-QDD’s continuous and peak torque values were measured using a high-impedance set-up and evaluated at 37.5 Nm and 89.9 Nm, respectively. The peak torque is significantly lower than the expected peak torque of 120 Nm based on the BLDC due to current limits on the C-QDD’s driver board. Table. II compares C-QDD to some of the actuators intended for legged robots with similar features. A low amplitude torque tracking bandwidth was also experimentally

TABLE I: C-QDD performance metrics

	C-QDD
Gear Type	Cycloidal
Gear Ratio	10
Continuous Torque (Nm)	37.5
Peak Torque (Nm)	89.9 (120)
No Load Speed [24V] (rpm)	128.6
Rated Power (W)	960
Output position Resolution (degree)	0.00219
Efficiency (%)	82.3
Torque Density (Nm/kg)	64.21 (85.71)
Actuator Inertia (kg·m²)	$5.01 \cdot 10^{-4}$
Weight (kg)	1.40
Backlash (arcmin)	7.03 ± 1.3
Static Back-drive Torque (Nm)	1.99
Dynamic Back-drive Torque (Nm)	1.36
Average Torque Ripple (Nm)	± 1.5
Torque Control Bandwidth [5 Nm] (Hz)	34.3
Position Control Bandwidth [45°] (Hz)	3.3
Position Control Bandwidth [5°] (Hz)	22.13

TABLE II: Efficiency and Torque Density Comparison

Metric	C-QDD	BEAR [35]	PULSE115-60 [22]	Lee et al. [5]
Peak Torque (Nm)	89.9	32	62.5	155.32
Mass (kg)	1.40	0.670	1.25	1.85
Gearing Ratio	10:1	10:1	5:1	11:1
Torque Density (Nm/kg)	64.2	47.7	50	83.7
Efficiency (%)	82.3	-	-	90

obtained and evaluated at 34.3 Hz. This was done through the high-impedance setup and by commanding a torque chirp signal to the actuator with a magnitude of 5 Nm.

B. C-QDD Backdrivability Performance

1) *Backlash*: The backlash of C-QDD was measured based on the method discussed in [36]. For this test, the C-QDD chassis was fixed to the bed with no load attached to its output. The actuator is first preloaded in the opposite direction, then the BLDC motor is gradually rotated until an output shaft motion is observed. A dial indicator with an accuracy of 0.0127 mm was used to identify when the output shaft moved. To account for inaccuracies in the manufacturing and assembly processes, this test was performed at six different locations of the output shaft, preloaded in both directions. The average backlash was calculated at 7.0 arcminutes with an uncertainty of ± 1.3 arcminutes. The backlash is comparable to other actuators designed for similar purposes, such as the one in [22].

2) *Static and Dynamic Backdriving Torque*: The torque needed to back-drive the C-QDD from the output was measured through the test setup shown in Fig. 5. The servo motor was used to back-drive the output of the C-QDD with a torque sensor rigidly fixed concentrically between the outputs of the actuator and servo. The static and dynamic backdriving torques—required to initiate and maintain motion, respectively—were both evaluated. The static and dynamic backdriving torques were observed at 1.99 Nm and 1.36 Nm, respectively. When compared to other QDD actuators, such as [22] and [37], which have backdriving torques of 0.37 Nm and 0.97 Nm, respectively, the backdriving force is higher, but comparable considering the C-QDD incorporates a higher gear-ratio and a considerably higher torque capability.

TABLE III: Comparison of Actuator Networks

Metric	PVA-GRU	PV-GRU	MLP (Tuned)	MLP (Baseline)
RMSE (Nm)	0.966	1.003	1.711	2.457
Variance (Nm)	0.923	0.853	2.903	3.622
Mean Error (Nm)	0.097	0.391	0.159	-0.19
Cycle Time (μ s)	1.492	3.095	0.716	0.221
Layers	4	4	3	3
History Size	30	30	24	3

*Cycle time refers to the execution time on the fastest available device: GPU for the GRU models and CPU for the MLP models.

C. Torque Estimation and Actuator Network Performance

To evaluate the Actuator Network’s performance for torque estimation, $\mathcal{X} = \{q, \dot{q}, \ddot{q}, \tau_q\}$ were collected on a single inverted pendulum setup using our C-QDD. The training data was generated using sinusoidal joint angle profiles with varying frequencies $f_q \in (0.3, 1.5)$ Hz, amplitude $\mathcal{A}_q \in (0.5, 1.5)$ rad, and initial position $q_{t=0} \in (0, 1)$ rad. The pendulum mass, $m_p \in \{1.14, 2.28\}$ kg was attached at varying locations on the pendulum bar, $r_p \in (0.25, 0.6)$ m, which represents various loads and inertia of the pendulum arm. The pendulum is allowed to make contact with a compliant wall, simulating the hybrid dynamics characteristics of legged robot motion.

1) *Actuator Net Performance Comparisons*: Fig. 6 graphs our torque estimation models, PVA-GRU and PV-GRU, against the ground truth. Root Mean Square Error (RMSE) and statistical torque estimation error distributions are shown in Fig. 6c. Table. III compiles RMSE and variances for all models.

As a baseline, a multilayer perceptron (MLP) used in [8] was trained on our dataset, and a tuned version of the MLP was also trained for further comparison. The tuned MLP and baseline MLP had an RMSE of 1.711 Nm and 2.457 Nm, respectively, demonstrating comparable results to the original implementation in [8], which is applied to a serial elastic actuator instead of a cycloid gear and operates under smaller torque ranges. Fig. 6 shows a visualization where all models agree with the ground truth for large-scale torque estimation. However, in Fig. 6b, the tuned MLP could not accurately capture small torque variation features, such as sinusoidal torque ripple with 0.6 Nm amplitude and 20 Hz frequency, showing a phase shift behavior of almost 180°.

On the other hand, the PVA-GRU model effectively leveraged the higher-order acceleration data to predict small amplitude and high-frequency variations accurately. As shown in Fig. 6b, the PVA-GRU estimated the torque ripple amplitude to be on average within 0.23 Nm, with a frequency of 17.61 Hz, compared to the ground truth value of 17.24 Hz, and a phase shift of less than 40°. Furthermore, the model demonstrated a significant improvement of 43.54% in RMSE and 68.21% in variance compared to the tuned MLP. Accurately capturing such torque nonlinearities is crucial for applications like RL simulations, where minor discrepancies in torque estimation can impact performance [7].

The PV-GRU torque estimations resemble a damped version of the ground truth output, with an average torque ripple prediction error of 0.71 Nm as shown in Fig. 6b. One notable

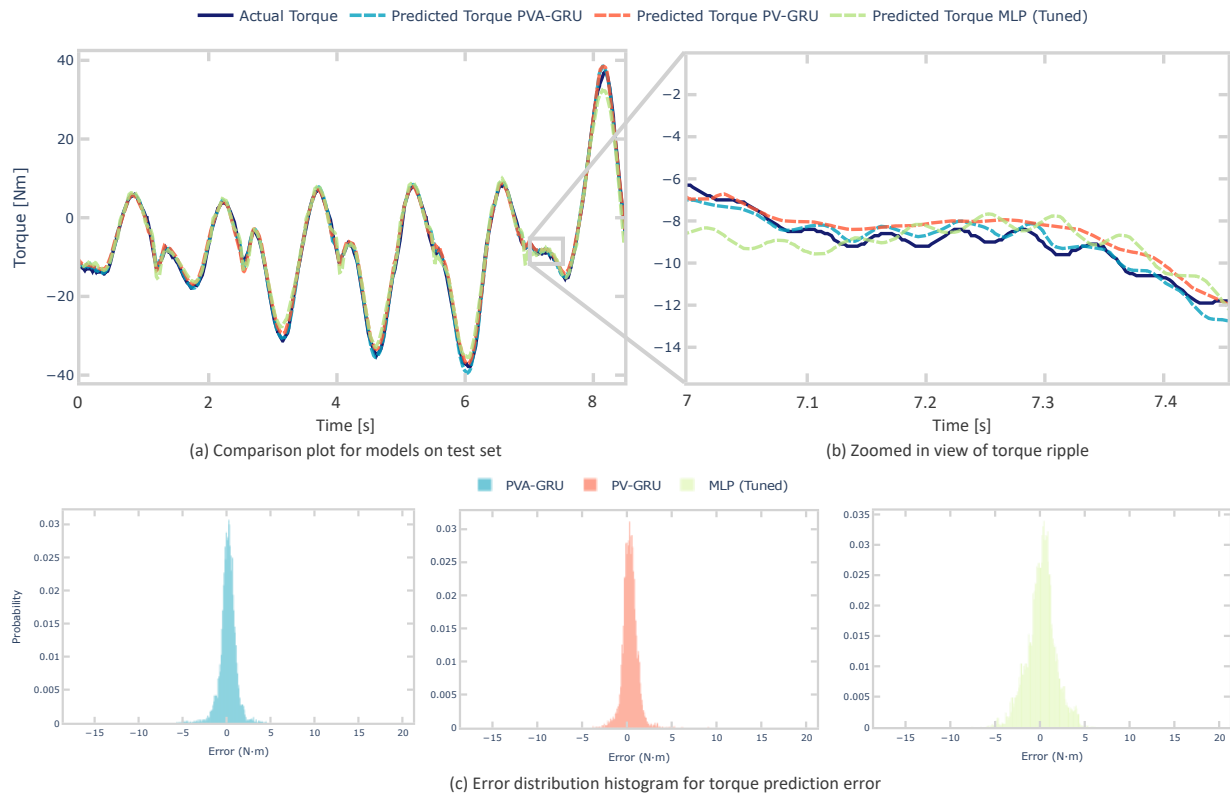


Fig. 6: The estimated torque and the ground truth torque

drawback of the PVA-GRU is that it relies on the noisier acceleration measurements. Thus, the predicted mean over time becomes less smooth compared to PV-GRU as shown in both Fig. 6a and the larger variance shown in Table. III. Nonetheless, statistically, the PVA-GRU has shown the highest accuracy overall. Hence, this supports that the PVA-GRU approach is effective for modeling actuator torque with detailed nonlinear features.

2) *Computational Cost*: In terms of computational cost, the PVA-GRU and PV-GRU run at $13.0 \mu\text{s}$ on CPU, while MLPs run at $<1.0 \mu\text{s}$. On GPU, the PVA-GRU and PV-GRU run at $1.5 \mu\text{s}$ and $3.1 \mu\text{s}$, respectively, including data transfer overhead between the GPU and CPU. Interestingly, the MLPs slow down to $4.227 \mu\text{s}$ on the GPU due to their simple network structure, where data transfer overhead becomes a bottleneck. These benchmarks were measured on an Intel Core i9-13900K CPU and an Nvidia RTX A2000 GPU on a test set of 16,000 data points.

This performance is sufficient for both simulation and hardware deployment, as demonstrated in [8]. The GRU-based architecture achieves real-time performance during live hardware verification, with average forward passes of $13 \mu\text{s}$ on CPU and $2 \mu\text{s}$ on GPU. Such processing speed is crucial for dynamic control tasks like legged locomotion, where fast response times ensure control loop frequencies above 1 kHz, necessary for torque control and quick terrain adaptation. For simulation, GPU acceleration significantly reduces training time, beneficial in RL environments where fast simulation accelerates control policy optimization across

numerous episodes and scenarios.

By incorporating acceleration into the state-space representation, the PVA-GRU model demonstrated its predictive capability, particularly in the presence of high-frequency nonlinearities, solidifying its utility in precision torque control for advanced robotic systems.

VI. CONCLUSION

This paper introduces a novel Cycloidal Quasi-Direct Drive actuator designed to meet the demanding needs of agile-legged robotics and climbing. The C-QDD actuator excels in torque density, mechanical rigidity, and low backlash, making it highly effective for high-load and dynamic environments commonly encountered in humanoid robots. Our GRU-based torque estimation framework demonstrates the ability to model the actuator's complex torque characteristics across high and low-amplitude motions without relying on direct torque sensing, potentially bridging the gap between simulation and real-world performance.

The hardware benchmarks have validated the C-QDD's superior backdrivability, torque density, and handling of dynamic loads, positioning it as a powerful solution for advanced robotic systems. Looking forward, our future research will focus on integrating this actuator and our torque estimation framework into force-aware planning [38], control [39], and reinforcement learning applications. We aim to further validate its performance in real-world applications, ultimately enhancing the agility and efficiency of legged robots in diverse and challenging scenarios.

REFERENCES

- [1] N. Kau, A. Schultz, N. Ferrante, and P. Slade, "Stanford doggo: An open-source, quasi-direct-drive quadruped," in *2019 International conference on robotics and automation*. IEEE, 2019, pp. 6309–6315.
- [2] G. Kenneally, A. De, and D. E. Koditschek, "Design principles for a family of direct-drive legged robots," vol. 1, no. 2, pp. 900–907. [Online]. Available: <http://ieeexplore.ieee.org/document/7403902/>
- [3] S. Seok, A. Wang, M. Y. Chuah, D. Otten, J. Lang, and S. Kim, "Design principles for highly efficient quadrupeds and implementation on the mit cheetah robot," in *2013 IEEE International Conference on Robotics and Automation*. IEEE, 2013, pp. 3307–3312.
- [4] T. Li, X. An, X. Deng, J. Li, and Y. Li, "A new tooth profile modification method of cycloidal gears in precision reducers for robots," *Applied Sciences*, vol. 10, no. 4, 2020. [Online]. Available: <https://www.mdpi.com/2076-3417/10/4/1266>
- [5] K. Lee, S. Hong, and J.-H. Oh, "Development of a lightweight and high-efficiency compact cycloidal reducer for legged robots," vol. 21, no. 3, pp. 415–425. [Online]. Available: <http://link.springer.com/10.1007/s12541-019-00215-9>
- [6] J. W. Sensinger and J. H. Lipsey, "Cycloid vs. harmonic drives for use in high ratio, single stage robotic transmissions," in *2012 IEEE International Conference on Robotics and Automation*. IEEE, pp. 4130–4135. [Online]. Available: <http://ieeexplore.ieee.org/document/6224739/>
- [7] R. Soni, D. Harnack, H. Isermann, S. Fushimi, S. Kumar, and F. Kirchner, "End-to-end reinforcement learning for torque based variable height hopping," in *2023 IEEE/RSJ International Conference on Intelligent Robots and Systems (IROS)*. IEEE, Oct. 2023. [Online]. Available: <http://dx.doi.org/10.1109/IROS55552.2023.10342187>
- [8] J. Hwangbo, J. Lee, A. Dosovitskiy, D. Bellicoso, V. Tsounis, V. Koltun, and M. Hutter, "Learning agile and dynamic motor skills for legged robots," *Science Robotics*, vol. 4, no. 26, p. eaau5872, 2019. [Online]. Available: <https://www.science.org/doi/abs/10.1126/scirobotics.aau5872>
- [9] T. Li, J. Zhou, X. Deng, J. Li, C. Xing, J. Su, and H. Wang, "A manufacturing error measurement methodology for a rotary vector reducer cycloidal gear based on a gear measuring center," vol. 29, no. 7, p. 075006, publisher: IOP Publishing. [Online]. Available: <https://iopscience.iop.org/article/10.1088/1361-6501/aac00a>
- [10] Y. Ye, R. B. Scharff, S. Long, C. Han, and D. Du, "Modelling of soft fiber-reinforced bending actuators through transfer learning from a machine learning algorithm trained from fem data," *Sensors and Actuators A: Physical*, vol. 368, p. 115095, 2024. [Online]. Available: <https://www.sciencedirect.com/science/article/pii/S0924424724000888>
- [11] Y. Tanaka, A. Schperberg, A. Zhu, and D. Hong, "Scaler-b: A multi-modal versatile robot for simultaneous locomotion and grasping," in *IEEE International Conference on Robotics and Automation @ 40 (ICRA@40)*.
- [12] Y. Tanaka, Y. Shirai, X. Lin, A. Schperberg, H. Kato, A. Swerdlow, N. Kumagai, and D. Hong, "Scaler: A tough versatile quadruped free-climber robot," in *2022 IEEE/RSJ International Conference on Intelligent Robots and Systems*, 2022, pp. 5632–5639.
- [13] Y. Tanaka, Y. Shirai, Z. Lacey, X. Lin, J. Liu, and D. Hong, "An under-actuated whippetree mechanism gripper based on multi-objective design optimization with auto-tuned weights," in *2021 IEEE/RSJ International Conference on Intelligent Robots and Systems*, 2021, pp. 6139–6146.
- [14] Y. Liu, J. Shen, J. Zhang, X. Zhang, T. Zhu, and D. Hong, "Design and control of a miniature bipedal robot with proprioceptive actuation for dynamic behaviors," in *2022 International Conference on Robotics and Automation (ICRA)*, 2022, pp. 8547–8553.
- [15] T. Suzuki, M. Bando, K. Kawaharazuka, K. Okada, and M. Inaba, "Saqiel: Ultra-light and safe manipulator with passive 3d wire alignment mechanism," *IEEE Robotics and Automation Letters*, vol. 9, no. 4, pp. 3720–3727, 2024.
- [16] G. A. Pratt and M. M. Williamson, "Series elastic actuators," in *Proceedings 1995 IEEE/RSJ International Conference on Intelligent Robots and Systems. Human Robot Interaction and Cooperative Robots*, vol. 1, 1995, pp. 399–406 vol.1.
- [17] B. Vanderborght, A. Albu-Schaeffer, A. Bicchi, E. Burdet, D. G. Caldwell, R. Carloni, M. Catalano, O. Eiberger, W. Friedl, G. Ganesh, M. Garabini, M. Grebenstein, G. Grioli, S. Haddadin, H. Hoppner, A. Jafari, M. Laffranchi, D. Lefeber, F. Petit, S. Stramigioli, N. Tsagarakis, M. Van Damme, R. Van Ham, L. C. Visser, and S. Wolf, "Variable impedance actuators: A review," *Robot. Auton. Syst.*, vol. 61, no. 12, p. 1601–1614, Dec. 2013. [Online]. Available: <https://doi.org/10.1016/j.robot.2013.06.009>
- [18] Y. Zhao, S. Lin, Z. Zhu, and Z. Jia, "A bipedal wheel-legged robot with high-frequency force control by quasi-direct drive: Design and experiments," in *2022 IEEE International Conference on Robotics and Biomimetics (ROBIO)*, 2022, pp. 58–63.
- [19] G. Kenneally, A. De, and D. E. Koditschek, "Design principles for a family of direct-drive legged robots," *IEEE Robotics and Automation Letters*, vol. 1, no. 2, pp. 900–907, 2016.
- [20] J. Luo, S. Ye, J. Su, and B. Jin, "Prismatic quasi-direct-drives for dynamic quadruped locomotion with high payload capacity," *International Journal of Mechanical Sciences*, vol. 235, p. 107698, 2022. [Online]. Available: <https://www.sciencedirect.com/science/article/pii/S0020740322005793>
- [21] A. Bajpai, C. Carrasquillo, J. Carlson, J. Park, D. Iyengar, K. Herrin, A. J. Young, and A. Mazumdar, "Design and validation of a versatile high torque quasidirect drive hip exoskeleton," *IEEE/ASME Transactions on Mechatronics*, vol. 29, no. 1, pp. 789–797, 2024.
- [22] C. A. Pérez-Díaz, I. Muñoz, D. Martín-Hernández, C. Candelozuluaga, I. Torres, J. Marsà, D. Sanz-Merodio, and M. López, "Design and experimental characterisation of a novel quasi-direct drive actuator for highly dynamic robotic applications," in *2024 IEEE International Conference on Robotics and Automation (ICRA)*, 2024, pp. 183–189.
- [23] P. L. García, S. Crispel, E. Saerens, T. Verstraten, and D. Lefeber, "Compact gearboxes for modern robotics: A review," vol. 7, p. 103. [Online]. Available: <https://www.frontiersin.org/article/10.3389/frobot.2020.00103/full>
- [24] M. Penčić, M. Čavić, and B. Borovac, "Development of the low backlash planetary gearbox for humanoid robots," *FME Transactions*, vol. 45, no. 1, 2017.
- [25] A. A. Hamza Tariq, Zhaksylyk Galym and C. Spitas, "Assessment of contact forces and stresses, torque ripple and efficiency of a cycloidal gear drive and its involute kinematical equivalent," *Mechanics Based Design of Structures and Machines*, vol. 52, no. 3, pp. 1304–1323, 2024. [Online]. Available: <https://doi.org/10.1080/15397734.2022.2144885>
- [26] T. G. Ling, M. F. Rahmat, and A. R. Husain, "System identification and control of an electro-hydraulic actuator system," in *2012 IEEE 8th International Colloquium on Signal Processing and its Applications*, 2012, pp. 85–88.
- [27] W. Zhao, J. P. Queraltá, and T. Westerlund, "Sim-to-real transfer in deep reinforcement learning for robotics: a survey," in *2020 IEEE Symposium Series on Computational Intelligence (SSCI)*, 2020, pp. 737–744.
- [28] A. Schperberg, Y. Tanaka, F. Xu, M. Menner, and D. Hong, "Real-to-sim: Predicting residual errors of robotic systems with sparse data using a learning-based unscented kalman filter," in *2023 20th International Conference on Ubiquitous Robots*, 2023, pp. 27–34.
- [29] W. Zhu, X. Guo, D. Owaki, K. Kutsuzawa, and M. Hayashibe, "A survey of sim-to-real transfer techniques applied to reinforcement learning for bioinspired robots," *IEEE Transactions on Neural Networks and Learning Systems*, vol. 34, no. 7, pp. 3444–3459, 2023.
- [30] L. Xu and Y. Yang, "Dynamic modeling and contact analysis of a cycloid-pin gear mechanism with a turning arm cylindrical roller bearing," *Mechanism and Machine Theory*, vol. 104, pp. 327–349, 2016. [Online]. Available: <https://www.sciencedirect.com/science/article/pii/S0094114X16301239>
- [31] C.-F. Hsieh, "Dynamics Analysis of Cycloidal Speed Reducers With Pinwheel and Nonpinwheel Designs," *Journal of Mechanical Design*, vol. 136, no. 9, p. 091008, 06 2014. [Online]. Available: <https://doi.org/10.1115/1.4027850>
- [32] J. Chung, C. Gulcehre, K. Cho, and Y. Bengio, "Empirical evaluation of gated recurrent neural networks on sequence modeling," 2014. [Online]. Available: <https://arxiv.org/abs/1412.3555>
- [33] L. N. Smith and N. Topin, "Super-convergence: Very fast training of neural networks using large learning rates," 2018. [Online]. Available: <https://arxiv.org/abs/1708.07120>
- [34] Z. Zhang, "Improved adam optimizer for deep neural networks," in *2018 IEEE/ACM 26th International Symposium on Quality of Service (IWQoS)*, 2018, pp. 1–2.
- [35] T. Zhu, J. Hooks, and D. Hong, "Design, modeling, and analysis of a liquid cooled proprioceptive actuator for legged robots," in *2019 IEEE/ASME International Conference on Advanced Intelligent*

- Mechatronics (AIM)*, vol. 2. IEEE, pp. 36–43. [Online]. Available: <https://ieeexplore.ieee.org/document/8868596/>
- [36] D. Gebler and J. Holtz, “Identification and compensation of gear backlash without output position sensor in high-precision servo systems,” in *IECON’98. Proceedings of the 24th Annual Conference of the IEEE Industrial Electronics Society (Cat. No. 98CH36200)*, vol. 2. IEEE, 1998, pp. 662–666.
- [37] S. Yu, T.-H. Huang, X. Yang, C. Jiao, J. Yang, Y. Chen, J. Yi, and H. Su, “Quasi-direct drive actuation for a lightweight hip exoskeleton with high backdrivability and high bandwidth,” vol. 25, no. 4, pp. 1794–1802. [Online]. Available: <https://ieeexplore.ieee.org/document/9095261/>
- [38] Y. Shirai, X. Lin, A. Schperberg, Y. Tanaka, H. Kato, V. Vichathorn, and D. Hong, “Simultaneous contact-rich grasping and locomotion via distributed optimization enabling free-climbing for multi-limbed robots,” in *2022 IEEE/RSJ International Conference on Intelligent Robots and Systems*. IEEE, 2022, pp. 13 563–13 570.
- [39] A. Schperberg, Y. Shirai, X. Lin, Y. Tanaka, and D. Hong, “Adaptive force controller for contact-rich robotic systems using an unscented kalman filter,” in *2023 IEEE-RAS 23rd International Conference on Humanoid Robots*, 2023.